Dynamics and specificity of cortical map reorganization after retinal lesions

Dimitrios V. Giannikopoulos and Ulf T. Eysel*

Department of Neurophysiology, Ruhr University Bochum, D-44780 Bochum, Germany

Communicated by Jon H. Kaas, Vanderbilt University, Nashville, TN, June 1, 2006 (received for review March 24, 2006)

Neurons in the mature visual cortex deprived of their normal retinotopic inputs by matched binocular retinal lesions are initially silenced but become reactivated with time when the ''blind'' cortical lesion projection zone (LPZ) is filled in by new suprathreshold visual responses. In an attempt to gain further insight into the dynamics of this process, we investigated in detail the spatiotemporal pattern of single-cell properties and recording probability during cortical reorganization up to 12 months after retinal lesions. In the early phases of filling in, a transient peak of hyperactivity moves from the border of the normal cortex into the LPZ and forms the leading edge of a functional reconnection process. In the course of this process hyperactive cells inside the LPZ develop ectopic receptive fields that are initially enlarged and regain orientation specificity. During the proceeding recovery, hyperactivity and receptive field size normalize, while the quality of orientation tuning remains reduced at longer distances inside the LPZ at all stages of recovery up to 1 year. Within the adult anatomical framework of cortical connectivity, the maximal lateral distance of reconnection is limited, and the probability to encounter spiking cells decreases with increasing distance inside the LPZ. However, this recording probability was significantly increased after 1 year.

binocular lesions | neuronal reorganization | visual cortex | adult cat

Retinal lesions cause a blind cortical region, the lesion projection zone (LPZ). Given enough time for recovery, an increasing number of supragranular cells inside the LPZ become progressively excitable, and new visual responses with displaced receptive fields (RFs) characterize a filling-in process (1–6). Provided that lesions are not too large, the filling in can be complete in experimental animals (1–6) and humans (7, 8). A certain reorganization of the retinotopic map already has been observed at the thalamic level in the lateral geniculate nucleus (LGN) of adult cats (9, 10), where monocular retinal lesions at 15–20° eccentricity result in topographical displacement of RFs up to 5° of visual angle (corresponding to 250 μm in the LGN). At the cortical level, comparable RF displacements after paracentral lesions indicate cortical reorganization over distances >2.5 mm (1, 3, 5). A short time after retinal lesions, cells with enlarged RFs are found at the border of the LPZ (3, 4). A reduction of the initially enlarged RF sizes (3) and a refinement in the main RF properties have been observed after completion of the long-term reorganization process (6). However, cortical reorganization was questioned on the basis of the permanently reduced metabolic signal of cytochrome oxidase activity in the LPZ of primates (11). More recently, a functional MRI (fMRI) study in monkeys revealed no shrinkage of the initially silent visual cortical region [blood oxygen level-dependent (BOLD)-defined LPZ] months after retinal lesions and concluded a lack of cortical reorganization (12). Here we present details about functional recovery and the process of visuotopic reorganization in the visual cortex at the single-cell level. Our findings consolidate the existence of cortical reorganization, highlight the spatiotemporal dynamics of the filling-in process, show a differential potential for recovery of simple and complex neuronal properties, and offer explanations for the discrepancy between imaging and single-cell data.

Results

Homonymous binocular retinal lesions of ≈10° in diameter were centered over both areae centrales (Fig. 1*A*) under light general anesthesia by using a xenon light photocoagulator. Recordings were performed after 2, 4, and 12 weeks and 1 year of survival in a visually rich environment. The shortest survival time, 2 weeks, provided enough time for decongestion of possible retinal edema before recordings. Neuronal activity was sampled from the supragranular layers down the medial bank through the LPZ and into normal area 17 by using a seven-electrode array (Fig. 1*B*). Retinotopic position, RF size, spontaneous and visually driven activity, and orientation tuning were carefully determined for each recorded cell (Fig. 1 *C* and *D*). Reorganized RFs belonging to cells inside the LPZ were always found clustering in the retina directly adjacent to the lesions and only became progressively displaced to more peripheral eccentricities when the electrodes moved into normally innervated cortex (Fig. 1 *B* and *C*). This basic phenomenon of topographic remapping was used to determine the border of the LPZ at the intersection of the regression lines of normal and postlesion eccentricities in dependence on recording distance down the medial bank (Fig. 2*A*). Interestingly, the probability of encountering spiking cells, which was constant in control animals, decreased progressively over a distance of ≈3 mm inside the LPZ, with comparable range and slope at survival times up to 3 months, but displayed a significant recovery after 1 year (Fig. 2*B*).

Cells inside the LPZ revealed increased spontaneous activity with significant peaks at 2 and 4 weeks, whereas at the same time spontaneous activity in the LPZ center changed from very low values at 2 weeks to normal values at 12 weeks and 1 year (Fig. 3*A*). The spatiotemporal pattern of activity highlights a wave of hyperactivity migrating with time from the LPZ border into the LPZ followed by attenuation toward normality (Fig. 3 *B* and *C*). The peak of spontaneous hyperactivity was located 1.5 mm inside the LPZ after 2 weeks and nearly 2.5 mm inside after 4 weeks (Fig. 3*B*). The filling-in with new visual responses (Fig. 3*C*) showed a peak of hyperexcitability congruent with the one observed for spontaneous activity, with the first well defined RFs ≈1 mm inside the LPZ after 2 weeks and 2 mm inside after 4 weeks. For the most recently reconnected cells at the leading edge and peak of the hyperexcitability after 2 and 4 weeks, no classical RFs could be determined, although full-field visual activation was very strong. After 12 weeks, when the observed hyperexcitability had disappeared, well defined RFs were found another 1 mm farther inside and finally ≈3.5 mm from the LPZ border 1 year postlesioning (Fig. 3*C*).

Conflict of interest statement: No conflicts declared.

Freely available online through the PNAS open access option.

Abbreviations: LPZ, lesion projection zone; RF, receptive field; fMRI, functional MRI; BOLD, blood oxygen level-dependent.

*To whom correspondence should be addressed. E-mail: eysel@rub.de.

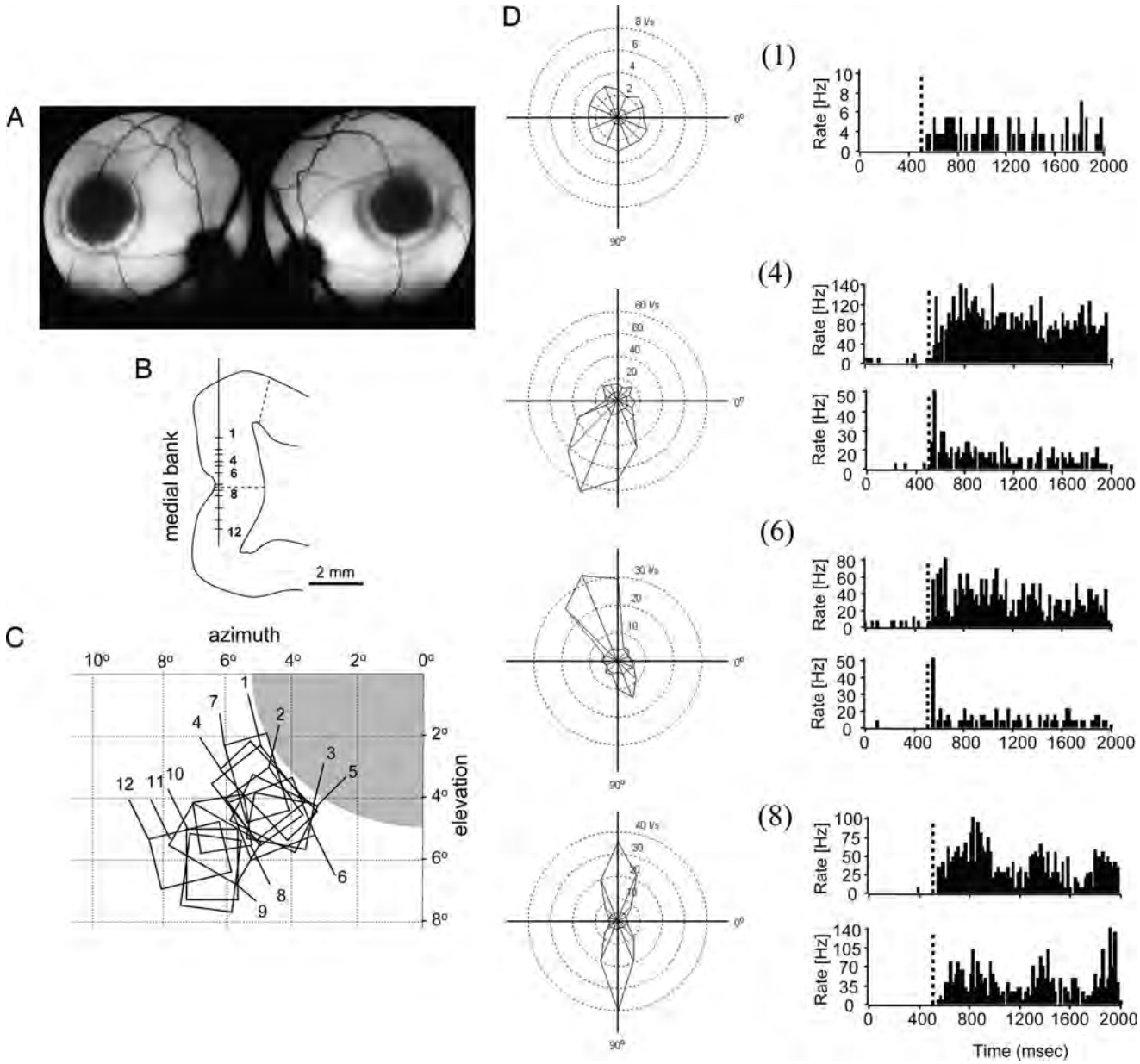

Fig. 1. Retinal lesions, RF topography, and single cell responses 4 weeks after lesion. (*A*) Fundus photographs of the left and right eyes of a cat with homonymous photocoagulator lesions of 10° diameter centered to the area centralis in both eyes. (*B*) Tangential recordings along the medial bank and sample recording sites (1–12) along a single penetration from an animal 4 weeks after lesion are shown on a schematic drawing of a frontal section. Dashed lines indicate the borders of the LPZ as determined for 10°-diameter lesions with zif/268 *in situ* hybridization (23, 25). (*C*) RF map of units recorded from the sample penetration shown in *B*. Retinal lesion is shown in gray. Units recorded in the LPZ have ectopic RFs at the retinal lesion border. (*D*) Polar diagrams of the visual evoked response for selected units (numbers indicated) and poststimulus time histograms of the responses to the preferred and null direction (stimulus onset at 500 ms). I/s, impulses per second.

Typically, RF width increases with increasing eccentricity in the visual field (13) and accordingly with increasing depth in tangential recordings down the medial bank (Fig. 4*A*, controls). The slope of this function was inverted when RF width was measured in the LPZ 2 and 4 weeks after retinal lesions, when RF width decreased at shorter distances from the LPZ border (Fig. 4*A*). The widest RFs were always the ones recorded farthest inside the LPZ and close to the peak of hyperexcitability at 2 and 4 weeks of survival time (Figs. 3*C* and 4*A*). After 12 weeks and 1 year, RFs found up to 3.5 mm inside the LPZ were, on average, indistinguishable in width from those of cells just outside the LPZ (Fig. 4*A*).

In contrast to RF width, orientation tuning did not significantly recover within 1 year after reconnection but remained dependent on distance from the LPZ border. Normal orientation tuning width is characterized by a continuous increase with increasing eccentricity (Fig. 4*B*, controls). However, when measured in cells participating in retinotopic remapping, the dependence of orientation tuning on recording depth was inverse after 2, 4, and 12 weeks and 1 year: The largest tuning width values were always found for the reconnected cells farthest inside the LPZ, whereas cells encountered closer to the border of the LPZ displayed increasingly tighter and finally normal tuning widths (Fig. 4*B*).

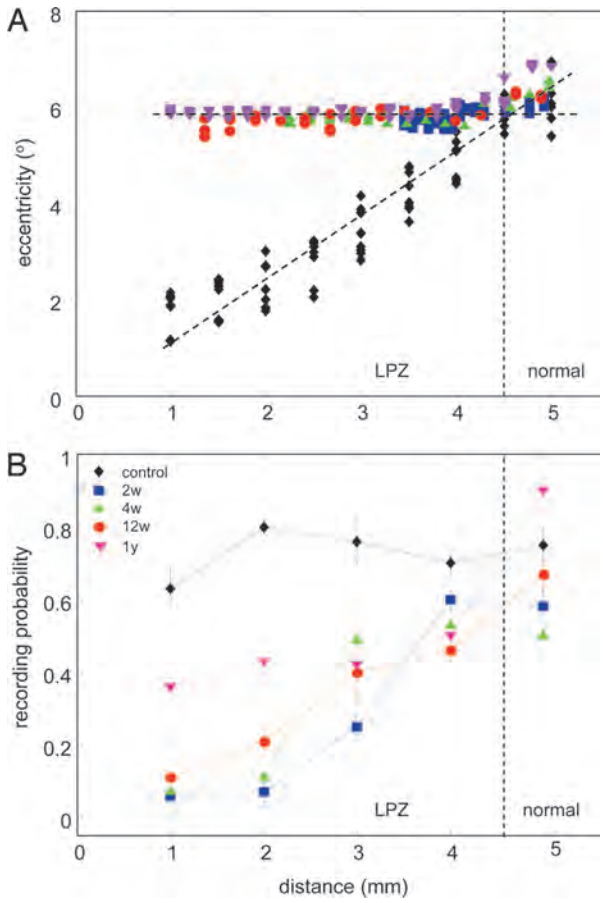

Fig. 2. RF positions and recording probability in control and lesioned animals. (*A*) Eccentricity of RF positions in the visual field from one control animal (black diamonds) and all experimental animals at 2 (blue square), 4 (green triangle), and 12 (red circle) weeks, and 1 year (magenta triangle) plotted in dependence of recording distance along the medial bank. The intersection between the regression lines indicates the border between LPZ and normal cortex. (*B*) The probability of recording spiking cells from positions separated by 150–300 μm within each 1 mm along the medial bank is shown for control, the 2-, 4-, and 12-week, and 1-year animals. All symbols and colors are as in *A*.

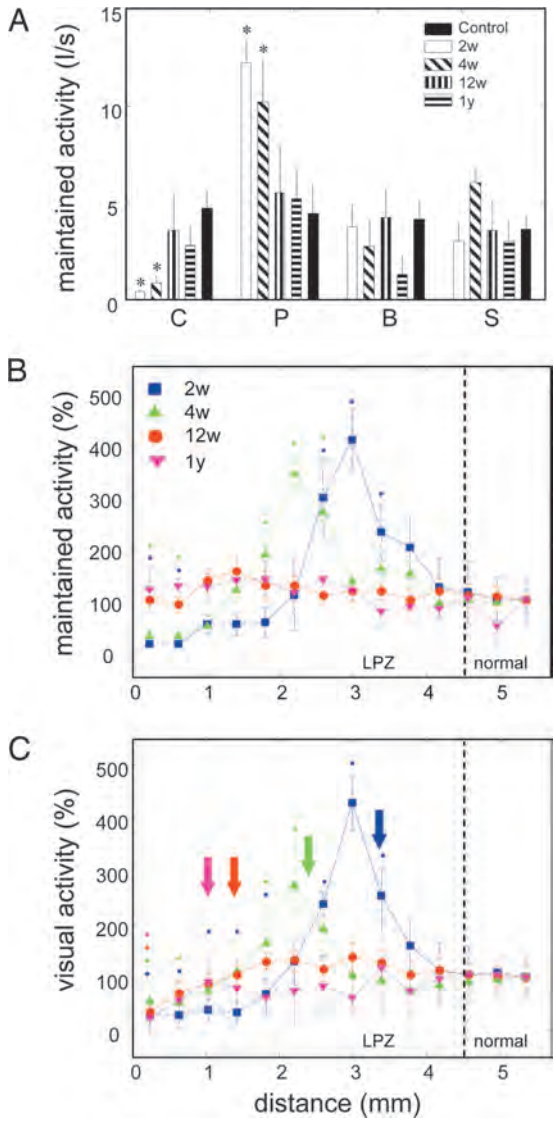

Fig. 3. Maintained and evoked activity in the LPZ at different recovery times. (*A*) Maintained activity in different characteristic zones of the LPZ. C, deafferented center; P, activity peak; B, border region of the LPZ; S, surround of LPZ. Controls recorded at corresponding eccentricities and results from different survival times are shown. Error bars are SEM. Asterisks indicate significant deviations from the normal surround ($P < 0.05$). I/s, impulses per second. (*B*) Normalized maintained activity as a function of increasing recording distance along the medial bank (see Fig. 1*B*). Activity outside the LPZ is set to 100% for each survival time. A peak of maintained activity is found progressively inside the LPZ at 2 and 4 weeks. Error bars and color coding of survival times are as in Fig. 2*B*. Color-coded dots indicate points where activity was significantly higher or lower compared with normal surround at respective survival times ($P < 0.05$). (*C*) Normalized maximal response to a drifting grating of preferred orientation and direction of motion. Normalization, color coding, and symbols are as in *B*. Color-coded arrows indicate the position of the first well defined RFs for different survival times.

Discussion

The cell properties followed in this study became adult-like by the end of the respective critical periods 8–12 weeks postnatal (14) when RF width reached adult-like values (15) and cells gained normal orientation specificity (15, 16). After homonymous retinal lesions in adulthood, the affected visual cortical cells are functionally disconnected and lose visual excitability (1–6). As shown by earlier work (1–6) and the present study, topographic reorganization takes place with time in the cortical LPZ. These results have been questioned on the basis of a long-term fMRI study in monkeys that failed to reveal any recovery of the cortical hemodynamic signal (12), although multiunit recordings performed at the end of the fMRI experiments after 7.5 months showed the characteristic RF topography with "pile-up" of RFs and visual responses in the LPZ such as those usually seen after cortical reorganization (1–6).

The discrepancies between the hemodynamic signal and single-cell recordings seem to reflect the selection of late vs. early phases of spiking activity in response to repetitive stimuli and differences in the definition of the LPZ. Neural responses and BOLD signal are separated in the temporal domain by an order of magnitude, and the strong early phase of multiunit activity (<2 s) in response to visual stimulation does not correlate well with the BOLD fMRI response (17). This unavoidably results in fMRI rejecting areas with shorter-lasting visual responses such as those present in the BOLD-defined LPZ center 7.5 months after retinal lesions (12). Here we have analyzed the first 1.5 s after stimulus onset, a time window that contains the most significant first 150–300 ms of neuronal information processing in the visual cortex (18, 19), as well as the maximal range of late event-related computations (20). Reorganization and subtle changes of RF properties within the LPZ were

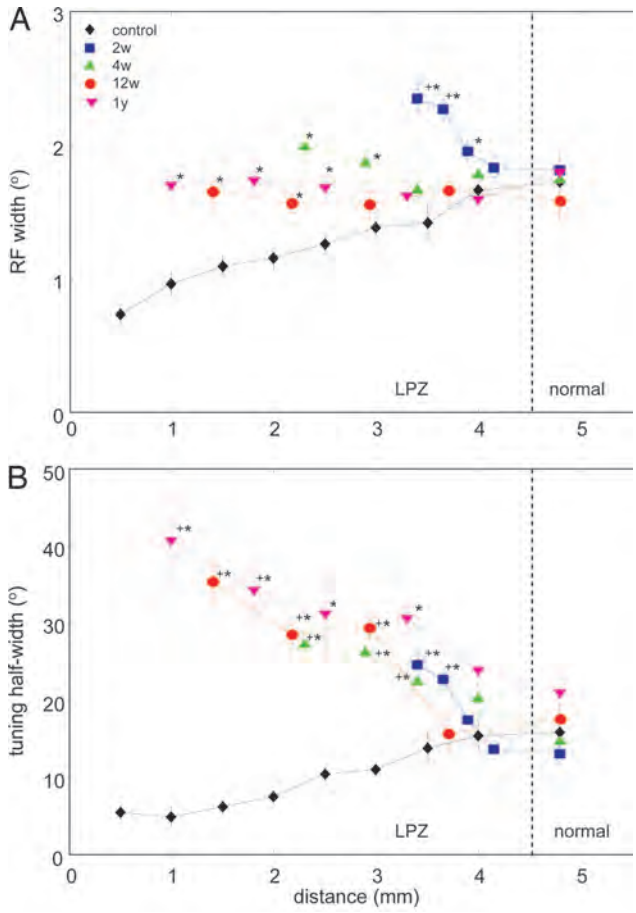

Fig. 4. Degree and limits of RF width and orientation tuning recovery. (*A*) RF widths from all recovery periods compared with normal RF widths recorded at corresponding eccentricities in control animals. Recording distance is defined as in Fig. 3*B*. Statistically significant differences at the 5% level are indicated by *; + indicates significant differences of RFs in the LPZ from those in the normal surround at each given survival time (color coding is as in Figs. 2 and 3). Error bars are SEM. (*B*) Orientation tuning half-width with increasing recording distance along the medial bank and eccentricity in the visual field. For explanation see *Results*. Color coding and symbols for significance are as in *A*.

expressed in this early activity that showed strong attenuation only for nonoptimal stimuli (Fig. 1*D*).

The border of the LPZ is topographically defined in single-cell studies as the cortical projection of RFs from the border of the retinal lesion, whereas in the fMRI study (12) the border of the LPZ was defined by the absence of a change in the BOLD signal during visual stimulation. The BOLD fMRI signal has been described as a powerful tool for visualizing input and local processing rather than spiking output in a given cortical region (17). Consequently, after the occurrence of retinal lesions, users of this tool are prone to underestimate (by at least 3–4 mm) the size of the deafferented area, the LPZ, because of the subthreshold lateral activation maintained via horizontal inputs (21) that also causes the comparatively large cortical point spread function observed with optical imaging of intrinsic signals (22).

Here we have attempted to compute an unbiased recording probability in dependence on the distance from the border of the LPZ by defining fixed recording positions without searching for spiking cells. The range and slope of the declining recording probability does not significantly change in the first months but clearly increases after 1 year. Both the recording probability decreasing from the border shown here (Fig. 2*B*) and the decreasing BOLD coherence observed with fMRI (12) might reflect the decreasing density (23) of the spatially limited lateral excitatory innervation (24) in the cortical region devoid of direct thalamocortical inputs and, hence, indicate the border of the single-cell-defined LPZ that undergoes reorganization of suprathreshold responses (21). After 1 year the recording probability far inside the LPZ recovered to ≈40%, indicating that reorganization does not remain restricted to a minority of cells. This late increase might be related to terminal sprouting of intracortical horizontal fibers only observed later than 8 months after retinal lesioning within the LPZ (24).

Further doubt of cortical reorganization was derived from another indirect measure of activity, the metabolic marker cytochrome oxidase, indicating long-term decrease of activity in the LPZ (11). However, like in fMRI, the degree of activity does not predict specificity and quality of responses. On the other hand, the expression of several molecular markers suggests synaptic plasticity and reorganization in the same location and time. Long-term up-regulation of synapsin I and neurotrophins was observed in the LPZ persisting after an early onset for >1 year (25). During the early phase of functional reorganization after retinal lesions in the adult cat, glutamic acid decarboxylase (GAD) immunoreactivity is down-regulated (26) in the neuropil of the LPZ, whereas a peak of up-regulated glutamate immunohistochemistry migrates with time into the LPZ (27), in parallel with the peak of hyperexcitability described here. This imbalance of reduced inhibition and increased excitation can provide a favorable environment for synaptic plasticity, such as that present in early postnatal life when GABAergic inhibition is weak or even inverted to excitation (28, 29). At this time, excitatory transmission prevails, and long-term potentiation as a sign of synaptic plasticity is strongly expressed (30). We hypothesize that lateral excitation, supernormal excitability, and synaptic use are the primary mechanisms that lead to reconnection and filling-in via horizontal cortical fiber systems after retinal lesions in our experiments. Indeed, long-term potentiation has been observed at horizontal inputs in the adult cat visual cortex (31), and horizontal fibers have shown late anatomical signs of plasticity after retinal lesions (23). Further support of our hypothesis comes from the increased phosphorylation of the α-subunit of Ca^{2+}/calmodulin-dependent protein kinase II observed in the LPZ of adult cats 2 and 4 weeks after lesioning (32). Use-dependent plasticity in early postnatal development is obviously coupled to up-regulation of $GABA_A$ receptor function (33); likewise, the refinement of RF size observed in the LPZ is accompanied by up-regulation of the GABAergic system with GAD immunohistochemistry restored to normal in the LPZ (26) and increased GABA levels in the surround (34).

Finally, we observed an interesting difference in recovery between RF width and orientation tuning quality. Whereas RF width returned to normal within 3 months, orientation tuning was found to be significantly decreased at distances >1 mm inside the LPZ, and it deteriorated with increasing distance from the border irrespective of recovery time. This might reflect the different neuronal computations that govern RF size and orientation tuning after reorganization. RF size might be simply controlled by adjusting the balance between excitation and inhibition (35, 36). However, because cells in the LPZ permanently lack the aligned (37, 38) or orientationally biased (39) thalamocortical inputs, their orientation tuning might deteriorate with distance from normal cortex because of the necessity of step-by-step integration of nonoptimally tuned lateral inputs.

Materials and Methods

Subjects and Cells. Eleven young adult cats were used [age, >8 (average of 13.3) months, 3.5–7.1 kg, mixed gender]: eight received binocular retinal lesions and three served as normal

controls. All procedures were in accordance with the German Animal Welfare Act of 1998.

Single-unit recordings were made from a total of 763 cells in area 17 of the adult cat [192 control units and 571 units from animals with retinal lesions at different survival times (74 at 2 weeks, 163 at 4 weeks, 136 at 12 weeks, and 198 at 1 year)].

Retinal Lesions. Homonymous central retinal lesions were produced under ketamine (20–30 mg/kg, i.m.) and xylazine hydrochloride (3 mg/kg, i.m.) anesthesia. Nictitating membranes were retracted with phenylephrine hydrochloride (5%), and pupil size was stabilized with atropine sulfate (1%). Lesions (LOG-2 xenon light photocoagulator, Clinitex, Denver, CO) had ≈10° diameter, were centered over the area centralis (documented by fundus photography), and destroyed all retinal layers. Recovery periods of 2, 4, and 12 weeks and 1 year were allowed before recordings, each with two animals.

Animal Preparation. For initial surgery (tracheotomy and femoral artery catheterization), cats were anesthetized as described above. Throughout the experiments, anesthesia was maintained by respiration with halothane (0.5–0.8%) in a mixture of N_2O/O_2 (70:30). Continuous infusion (6 ml/h) of Ringer's solution containing alcuronium chloride (0.06 mg/kg per h) and glucose (1.25%) provided paralysis and nutrition. Pressure points and wound margins were locally anesthetized (xylocaine gel, 2%). Temperature (38.5°C) and end-tidal CO_2 (3.8–4.2%) were kept constant, and systemic blood pressure and pulse rate were monitored continuously for adjustment of the level of anesthesia. Animals were fixed in a stereotaxic frame, and a craniotomy was performed (Horsley–Clarke coordinates, A5 to P5 and L0 to L9), exposing the visual cortex of the right hemisphere including the midline. After durotomy, a plastic chamber with a transparent film for replacing the dura was positioned inside the craniotomy for inspection and penetration. The chamber was fixed with bone wax.

Tapetal reflection images were used to correct for a viewing distance of 57 cm. Retinal lesions (appearing as dark pigmented areas), optic disks, and characteristic blood vessels were plotted as landmarks onto a tangent screen and monitored regularly to track any residual eye movements.

Recording and Visual Stimulation. A linear array (Eckhorn system, Thomas Recording, Giessen, Germany) of seven independently controlled microelectrodes (interelectrode spacing of 305 μm) was oriented mediolaterally at AP0 for tangential recordings down the medial bank. Electrodes were individually advanced through the LPZ into the normal cortex. Visual evoked and spontaneous activity was recorded at fixed steps every 150–300 μm over the full distance of each penetration, and data were pooled from the supragranular layers (three most medial active electrodes). The recording probability (P) describes the probability of recording a spiking cell at each recording position within 1 mm of each of the active electrodes [P = number of recorded cells)/(number of electrodes × number of steps)]. In each experiment, one to four penetrations were made between Horsley–Clarke coordinates AP0 and P4. Extracellular single-unit activity was amplified, high-pass filtered, digitized, and stored for offline analysis. Spikes were isolated by voltage thresholding and sorted online/offline by using a spike-clustering tool (BRAINWARE, version 7.301; TDT, Alachua, FL).

Stimuli were displayed on a video monitor (57-cm viewing distance, screen resolution of 800 × 600 pixels, vertical refresh rate of 120 Hz). Square-wave gratings of different orientation were used for visual stimulation. Stimulus parameters were manually adjusted to fit the properties of the recorded cell. Computer-controlled trials aided in further optimizing stimulation parameters. Ranges used were as follows: orientation, 0–180°; direction, 0–360°; spatial frequency, 0.2–0.7 cycles per °; and temporal frequency, 1–2 Hz.

Retinotopy. The extent of cortical reorganization was determined by plotting each RF onto a tangent screen with drawings of retinal landmarks and the outline of the retinal lesions. Recordings down the medial bank of control animals revealed RFs systematically shifting laterally away from the area centralis. In contrast, in lesioned animals there was no systematic RF shift; instead all neurons encountered in the LPZ had displaced RFs clustering at the border of the retinal lesion. The extent of the reorganized part of the LPZ was marked to start with the first clearly delimited RF inside the LPZ, whereas the first clear shift in RF location away from the border of the retinal lesions was taken as the LPZ border. RF boundaries were determined qualitatively with small bar-shaped light stimuli and were hand-plotted as rectangles. Distance (d, in cm) between the geometric center of the RF and foveal projection point on the tangent screen 57 cm in front of the cat's eyes was converted to degrees eccentricity (φ) by using the formula $\varphi = \arctan d/57$.

Data Analysis and Evaluation. To quantify changes in cortical excitability introduced by our retinal lesions, we recorded responses to monocularly presented full-field drifting square-wave gratings [0–180°; step size of 22.5°, random order, drifting in one direction for recording periods of 2 s (500 ms blank, 1,500 ms of visual stimulation) separated by intervals of 500 ms]. Spontaneous activity profiles were obtained at constant background illumination. Neurons were recorded for 5–10 min to produce poststimulus time histograms for each stimulus condition. Direction and orientation tuning curves were computed. Orientation half-bandwidth was measured at a response level equal to 66% of the maximum response amplitude. The visual evoked response (mean spike rate, in impulses per second) was computed from the period of stimulus presentation (1.5 s). The resulting evoked and spontaneous activity profiles for the different recovery periods (2, 4, and 12 weeks and 1 year) were compared by normalizing the responses with respect to the responses of neurons located in normal cortex outside the LPZ. Significance was tested by using Student's t test ($P < 0.05$).

This work was supported by Deutsche Forschungsgemeinschaft Grant SFB 509 TP C4 and Bundesministerium für Bildung und Forschung (Federal Ministry of Education and Research) Grant 01GI 9913.

1. Kaas, J. H., Krubitzer, L. A., Chino, Y. M., Langston, A. L., Polley, E. H. & Blair, N. (1990) *Science* **248,** 229–231.
2. Heinen, S. J. & Skavenski, A. A. (1991) *Exp. Brain Res.* **83,** 670–674.
3. Gilbert, C. D. & Wiesel, T. N. (1992) *Nature* **356,** 150–152.
4. Chino, Y. M., Kaas, J. H., Smith, E. L., III, Langston, A. L. & Cheng, H. (1992) *Vision Res.* **32,** 789–796.
5. Gilbert, C. D. (1992) *Neuron* **9,** 1–13.
6. Chino, Y. M., Smith, E. L., Kaas, J. H., Sasaki, Y. & Cheng, H. (1995) *J. Neurosci.* **15,** 2417–2433.
7. Gerrits, H. J. & Timmerman, G. J. (1969) *Vision Res.* **9,** 439–442.
8. Zur, D. & Ullman, S. (2003) *Vision Res.* **43,** 971–982.
9. Eysel, U. T., Gonzáles-Aguilar, F. & Mayer, U. (1981) *Exp. Brain Res.* **41,** 256–263.
10. Eysel, U. T. (1982) *Nature* **299,** 442–444.
11. Horton, J. C. & Hocking, D. R. (1998) *J. Neurosci.* **18,** 5433–5455.
12. Smirnakis, S. M., Brewer, A. A., Schmid, M. C., Tolias, A. S., Schuz, A., Augath, M., Inhoffen, W., Wandell, B. A. & Logothetis, N. K. (2005) *Nature* **435,** 300–307.
13. Albus, K. (1975) *Exp. Brain Res.* **24,** 159–179.
14. Daw, N. W. (1995) *Visual Development* (Plenum, New York).
15. Braastad, B. O. & Heggelung, P. (1985) *J. Neurophysiol.* **53,** 1158–1178.
16. Frégnac, Y. & Imbert, M. (1984) *Physiol. Rev.* **64,** 325–434.
17. Logothetis, N. K., Pauls, J., Augath, M., Trinath, T. & Oeltermann, A. (2001) *Nature* **412,** 150–157.
18. Gershon, E. D., Wiener, M. C., Latham, P. E. & Richmond, B. J. (1998) *J. Neurophysiol.* **79,** 1135–1144.

19. Muller, J. R., Metha, A. B., Krauskopf, J. & Lennie, P. (2001) *J. Neurosci.* **21,** 6978–6990.
20. Makeig, S., Westerfield, M., Jung, T.-P., Covington, J., Townsend, J., Sejnowski, T. J. & Courchesne, E. (1999) *J. Neurosci.* **19,** 2665–2680.
21. Calford, M. B., Chino, Y. M., Das, A., Eysel, U. T., Gilbert, C. D., Heinen, S. J., Kaas, J. H. & Ullman, S. (November 10, 2005) *Nature*, 10.1038/nature04359.
22. Das, A. & Gilbert, C. D. (1995) *Nature* **375,** 780–784.
23. Kisvárday, Z. F., Tóth, E., Rausch, M. & Eysel, U. T. (1997) *Cereb. Cortex* **7,** 605–608.
24. Darian-Smith, C. & Gilbert, C. D. (1994) *Nature* **368,** 737–740.
25. Obata, S., Obata, J., Das, A. & Gilbert, C. D. (1999) *Cereb. Cortex* **9,** 238–248.
26. Rosier, A. M., Arckens, L., Demeulemeester, H., Orban, G. A., Eysel, U. T., Wu, Y. J. & Vandesande, F. (1995) *J. Comp. Neurol.* **359,** 476–489.
27. Arckens, L., Schweigart, G., Qu, Y., Wouters, G., Pow, D. V., Vandesande, F., Eysel, U. T. & Orban, G. (2000) *Eur. J. Neurosci.* **12,** 4222–4232.
28. Guo, Y., Kaplan, I. V., Cooper, N. G. & Mower, G. D. (1997) *Brain Res. Dev. Brain Res.* **103,** 127–141.
29. Lin, M. H., Takahashi, M. P., Takahashi, Y. & Tsumoto, T. (1994) *Neurosci. Res.* **20,** 85–94.
30. Fox, K. (1995) *Neuron* **15,** 485–488.
31. Hirsch, J. A. & Gilbert, C. D. (1993) *J. Physiol. (London)* **461,** 247–262.
32. Van den Bergh, G., Eysel, U. T., Vandenbussche, E., Vandesande, F. & Arckens, L. (2003) *Neuroscience* **120,** 133–142.
33. Hensch, T. K. & Stryker, M. P. (2004) *Science* **303,** 1678–1681.
34. Massie, A., Cnops, L., Smolders, I., Van Damme, K., Vandenbussche, E., Vandesande, F., Eysel, U. T. & Arckens, L. (2003) *Brain Res.* **976,** 100–108.
35. Hirsch, J. A. & Gilbert, C. D. (1991) *J. Neurosci.* **11,** 1800–1809.
36. Worgotter, F., Suder, K., Zhao, Y., Kerscher, N., Eysel, U. T. & Funke, K. (1998) *Nature* **396,** 165–168.
37. Hubel, D. H. & Wiesel, T. N. (1962) *J. Physiol. (London)* **160,** 106–154.
38. Ferster, D., Chung, S. & Wheat, H. (1996) *Nature* **380,** 249–252.
39. Vidyasagar, T. R., Pei, X. & Volgushev, M. (1996) *Trends Neurosci.* **19,** 272–277.